IOPscience iopscience.iop.org

Home Search Collections Journals About Contact us My IOPscience

Accuracy of dynamic patient surface monitoring using a time-of-flight camera and B-spline modeling for respiratory motion characterization

This content has been downloaded from IOPscience. Please scroll down to see the full text.

2012 Phys. Med. Biol. 57 4175

(http://iopscience.iop.org/0031-9155/57/13/4175)

View the table of contents for this issue, or go to the journal homepage for more

Download details:

IP Address: 130.132.173.203
This content was downloaded on 14/09/2015 at 15:36

Please note that terms and conditions apply.

IOP PUBLISHING PHYSICS IN MEDICINE AND BIOLOGY

Phys. Med. Biol. **57** (2012) 4175–4193 doi:10.1088/0031-9155/57/13/4175

Accuracy of dynamic patient surface monitoring using a time-of-flight camera and B-spline modeling for respiratory motion characterization

T Wentz[1,3], H Fayad[1], J Bert[1], O Pradier[1,2], J F Clement[1], S Vourch[1,2], N Boussion[1,2] and D Visvikis[1]

[1] INSERM, UMR1101, LaTIM, CHRU Morvan, Brest F-29200, France
[2] Radiotherapy Department, CHRU Morvan, Brest F-29200, France

E-mail: thomas.wentz@telecom-bretagne.eu

Received 20 October 2011, in final form 13 April 2012
Published 8 June 2012
Online at stacks.iop.org/PMB/57/4175

Abstract

Time-of-flight (ToF) camera technology provides a real-time depth map of a scene with adequate frequency for the monitoring of physiological patient motion. However, dynamic surface motion estimation using a ToF camera is limited by issues such as the raw measurement accuracy and the absence of fixed anatomical landmarks. In this work we propose to overcome these limitations using surface modeling through B-splines. This approach was assessed in terms of both motion estimation accuracy and associated variability improvements using acquisitions of an anthropomorphic surface phantom for a range of observation distances (0.6–1.4 m). In addition, feasibility was demonstrated on patient acquisitions. Using the proposed B-spline modeling, the mean motion estimation error and associated repeatability with respect to the raw measurements decreased by a factor of 3. Significant correlation was found between patients' surfaces motion extracted using the proposed B-spline approach applied to the ToF data and the one extracted from synchronized 4D-CT acquisitions as the ground truth. ToF cameras represent a promising alternative for contact-less patient surface monitoring for respiratory motion synchronization or modeling in imaging and/or radiotherapy applications.

(Some figures may appear in colour only in the online journal)

1. Introduction

Respiratory motion is an important source of image degradation and artifacts, compromising accurate quantitation in thoracic and abdominal imaging studies (Boucher *et al* 2004). In

[3] Author to whom any correspondence should be addressed.

 © 2012 Institute of Physics and Engineering in Medicine

addition, the uncertainties resulting from breathing hinder the localization of internal structures in these body regions, and are still today a major limitation in external beam radiotherapy treatment planning and delivery. Variable levels of motion have been reported for different organs affected by respiration. Studies have shown that the magnitude of displacements of the lungs' lower regions is significantly larger than the ones of the upper regions (5 ± 2 cm versus 0.9 ± 0.4 cm) (Plathow *et al* 2004). At the level of the abdomen, the largest movements are observed along the cranio-caudial direction for pancreas and liver (23 ± 15.9 mm and 24.4 ± 16.4 mm, respectively) and even the smallest displacements affecting the kidneys reach 17 ± 7 mm (Bussels *et al* 2003). Respiratory gating techniques have been introduced to reduce the respiratory motion impact thanks to monitoring a patient's breathing in order to synchronize the image acquisition process (Nehmeh *et al* 2004) or the radiotherapy beam delivery (Kubo and Hill 1996) with the respiration. Within the context of such synchronization, different approaches and associated technologies have been proposed for monitoring a patient's respiratory motion, such as for example passive infrared reflective markers placed on the patient's torso (Mageras *et al* 2001, Wagman *et al* 2003), pressure-sensitive belts (Bundschuh *et al* 2007) or electromagnetic markers (Smith *et al* 2009).

While respiratory gating may be used to reduce the impact of motion, an alternative approach involves the prediction of internal organ motion through the use of external motion tracking. Several studies have indicated that external one-dimensional (1D) surrogate measures of respiratory motion may correlate with internal structures' and tumor motion (Tsunashima *et al* 2004, Beddar *et al* 2007, Kanoulas *et al* 2007). However, such a 1D and spatially restricted respiratory signal may be insufficient for the prediction of internal organ motion, considering the variability in individual patient anatomy and specific motion, in combination with the different magnitudes of displacement associated with different regions of a patients' external surface. The motion of the patient's surface during a complete respiratory cycle can reach 10 mm (respectively, 3 mm) in the antero-posterior direction and 3 mm (respectively, 2 mm) in the cranio-caudal direction in the abdominal (respectively, thoracic) area. It has been suggested that the position of the external surrogates and the acquisition protocol used can increase or decrease the observed internal-external correlation in an arbitrary fashion (Wu *et al* 2008).

In order to minimize such issues and overcome the observed variability, a complete patient surface motion characterization could allow the extraction of complementary information compared to a restrictive 1D respiratory signal. A few techniques allow the observation of a patient surface such as the use of structured light (Chen *et al* 2010) or stereoscopic methods (Vasquez *et al* 2009). In recent studies Spadea *et al* (2011) and Kauweloa *et al* (2012) used a structured light system (GateCT™, VisionRT, London, UK) for respiratory sensing and 4D-CT reconstruction. In these works a 1D respiratory signal extracted in a 20×20 mm^2 patient surface area was used for the 4D-CT respiratory motion synchronization. The fastest rate that has been reported for the entire surface capture using this technology is 1–1.7 frames per second (Peng *et al* 2010) and limited by the computational complexity of the correspondence search algorithm. More recently, Price *et al* (2012) have shown that the use of fast structured light surface system technology may be able to provide overall surface information with rates up to 23 Hz, albeit with an added complexity of a cumbersome calibration protocol. In addition, in this work only the accuracy of a static surface capture was assessed, while the dynamic information was only extracted using an ICP rigid body transformation which was not performed in real time.

An alternative technology recently developed is a 3D camera based on time-of-flight (ToF) technology. Such a camera provides a 3D distance map of a scene, thanks to the emission of light in the near infrared range, which actively illuminates the scene, followed by the capture of the reflected light (Oggier *et al* 2004). This technology offers certain advantages compared

to other surface observation techniques, allowing the monitoring of the whole patient surface sufficiently rapidly for real-time respiratory motion tracking and this without the need of any complicated calibration steps. The complete surface can be described by more than 25 000 3D points for each frame at an associated frame acquisition rate of up to 30 Hz. To date, the main applications for this technology have been in the detection of intrusion (Guomundsson *et al* 2008), driving assistance (Hsu *et al* 2006) or graphic-related applications (Kolb *et al* 2010). Previous attempts to use a ToF camera for respiratory motion monitoring have been restricted to evaluating the potential of such technology to provide 1D respiratory motion signals compared to those obtained with a pressure belt (Falie *et al* 2008, Penne *et al* 2008, Clement *et al* 2009).

Recently, the use of patient surface motion has been proposed for the development of intra-patient respiratory motion models and/or the personalization of a generic respiratory motion model that can be subsequently used either in 4D imaging or 4D therapy delivery applications (Fayad *et al* 2009). This study demonstrated that the use of complete surface characterization allows for improved accuracy in modeling patient-specific respiratory motion compared to the use of a 1D external respiratory signal. However, such an approach is clearly dependent on the availability of technology and associated surface modeling methodology capable of following patient surface changes as a function of intra-patient respiratory motion. Before the potential of the camera ToF technology can be realized within the context of interest, it is important to assess its accuracy in measuring patient surface displacements in real time. The real-time aspect is important for the eventual targeted applications such as for example respiratory motion management during radiotherapy treatment. A ToF camera provides a 3D point cloud describing the observed surface for each frame acquisition. During a dynamic acquisition, these successive 3D point clouds need to be associated with each other before they can be used to characterize and quantify the motion of a complete patient's surface. Such an association of the different time frames is complicated by the lack of anatomical landmarks in the measured patient surfaces. The main objective of this study was therefore to characterize the ToF camera performance improvement in measuring complete patient surface motion in real time using B-Spline modeling applied to the ToF raw data. The use of the B-Spline modeling approach for the surface motion extraction in real time is justified by the computational costs associated with surface motion extraction methods using deformable registration (Schaerer *et al* 2012).

The proposed approach was first validated regarding its accuracy and repeatability using acquisitions of an anthropomorphic torso phantom. The feasibility and potential impact of characterizing patients' entire external surfaces motion using the proposed technology and presented methodology was also investigated. This was carried out by comparing (a) the respiratory motion signals derived from the raw surface measurements, (b) the motion of different surface regions of interest (ROIs) extracted from skin segmentation on patient 4D-CT images with the motion characterized by the proposed approach on the same patient surface regions and (c) the use of the modeled camera surfaces relative to motion 1D amplitude information for the construction of a patient-specific motion model.

2. Materials and methods

2.1. ToF camera

The ToF camera provides a 3D distance map of a scene, based on the emission of light in the near infrared range (see figure 1). Each pixel of the CCD measures the light reflected by the illuminated object. The distance between the camera and the point of reflection can be deduced by a simple computation of the phase difference between the incoming light and

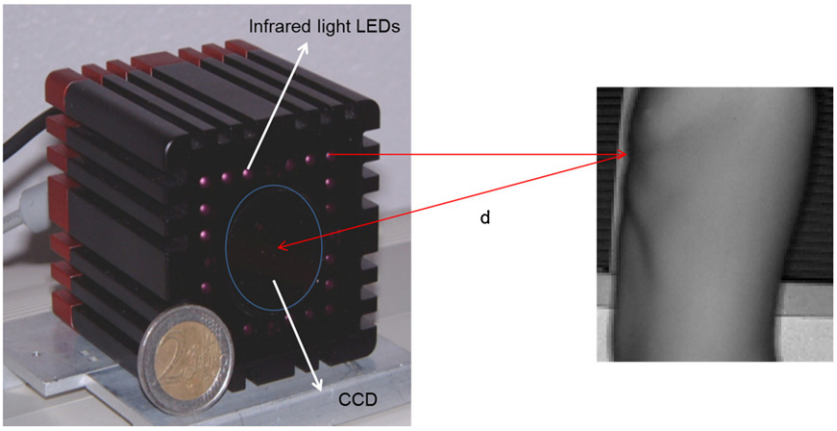

Figure 1. ToF camera and associated principle of operation.

Table 1. SwissRanger© 4000 camera (MESA Imaging^{TM}) technical characteristics.

Physical dimensions	65 × 65 × 68 mm^3
Resolution	176 × 144
Maximal acquisition rate	54 Hz
Measurement range	0.3 to 5 m
Nominal accuracy at 1 m or less	1% of the distance between the camera and the object
Repeatability at 2 m or less	<5 mm
Angular resolution	0.23°

the initially emitted one. The relation between the distance d and the phase difference Φ is given by equation (1).

$$d = \frac{\Phi^* c}{4^* \pi^* f}, \tag{1}$$

where c is the speed of light and f is the modulation frequency.

The physical characteristics of the SwissRanger© 4000 camera used in this work are given in table 1 (SR4000 User's manual 2012). This camera has several practical advantages, being fast (30 Hz maximum rate), portable and light, allowing for a surface observation within a large range of distance and frequency. According to the manufacturer's specification, the nominal accuracy decreases linearly between 0.3 and 1 m of the distance between the camera and the object (∼1% of the distance) and becomes stable at 1 cm for distances > 1 m. However, various processing schemes, such as filtering or averaging techniques, can be used to improve this accuracy. The acquisition rate depends on the integration time and can be tuned up to 30 Hz and the camera also offers an automatic exposure optimization to avoid saturation effects. Its angular resolution allows a field of view corresponding to a target area of ∼60 × 45 cm^2 at a distance of 80 cm, with a 3D point cloud (maximum of 25 000 points) describing the scene (∼3 × 3 mm^2 'pixel' size).

In this study, all acquisitions were performed with the highest modulation frequency (31 MHz) in order to provide the finest measurement possible. The acquisition frequency was 2 Hz for phantom experiments, constrained by the automatic exposure mode. For patient acquisitions, we restricted the acquisition frequency to 10 Hz in order to provide an efficient

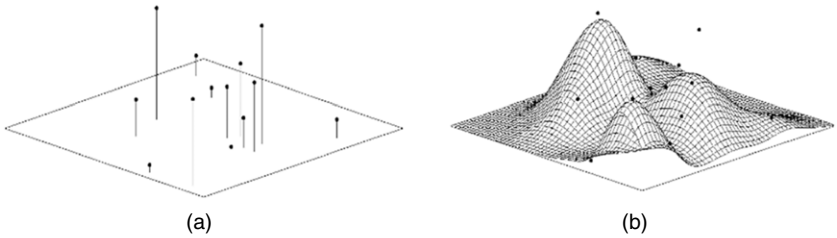

Figure 2. Surface representation using (a) scattered data and (b) modeling with B-splines.

binning (Brandner *et al* 2006, Dawood *et al* 2009). Since the respiratory cycle was divided in 22 bins, and a respiratory cycle is usually longer than 2 s, we considered 10 Hz as a good compromise between temporal sampling and exposure time length. Although multiple noise reduction acquisition modes are made available by the manufacturer, only default settings were used in this work.

2.2. Extraction of 3D motion vectors

The raw data points provided by the ToF camera are directly computed from the phase difference of the reflected light (see section 2.1). It is composed of 25 344 3D points (corresponding to the number of pixels in the CCD detector) describing illuminated surfaces on the camera's observation scene. The surfaces defined by the camera ToF acquired raw data points were modeled using a scattered data interpolation. Given a set $P_i = (x_i, y_i)$, $(i = 1, \ldots, n)$ of n irregularly distributed points over $\mathbb{R}^2$, and scalar values F_i associated with each point, satisfying $F_i = F(x_i, y_i)$ for some underlying function $F(x, y)$, an interpolating function $F^* \approx F(x, y)$ such that for $i = 1, \ldots, n$ is determined using equation (2).

$$F^*(x_i, y_i) = F_i. \tag{2}$$

Contrary to a homogeneous grid of points, the use of scattered data points does not allow easy and fast spatial averaging and filtering. It also provides locally non-homogeneous information along the surface. These issues associated with a grid of non-regular points were resolved by using a surface modeling through B-splines. The resulting B-spline function interpolating the scattered data can be considered as F^* in equation (2). The resulting function is considered as a piecewise union of splines and the generated control points form a grid of regular 3D points with resolution and position chosen by the user (see figure 2).

The complete motion of a surface during time can be characterized by the control points' motion through the successive frames. The first step in this process is the transformation of the camera's spatial reference frame to that of the examination table (see figure 3(a)). The examination table reference frame is determined by its associated plane and an arbitrarily positioned origin. Hence by comparing the displacement of the patient's external surface relative to the table reference (e.g. through the comparison of the successive surfaces' depth variations), the motion of the observed surface can be determined as the motion of the control points relative to the same reference, namely the examination table reference frame (see figure 3(b)).

Given two sets $B_{i,j} = (x_{i,j}, y_{i,j})$ and $B_{i,j+1} = (x_{i,j+1}, y_{i,j+1})$ of n' regularly distributed points over $\mathbb{R}^2$ describing the same surface at consecutive time points j and $j + 1$, and scalar values

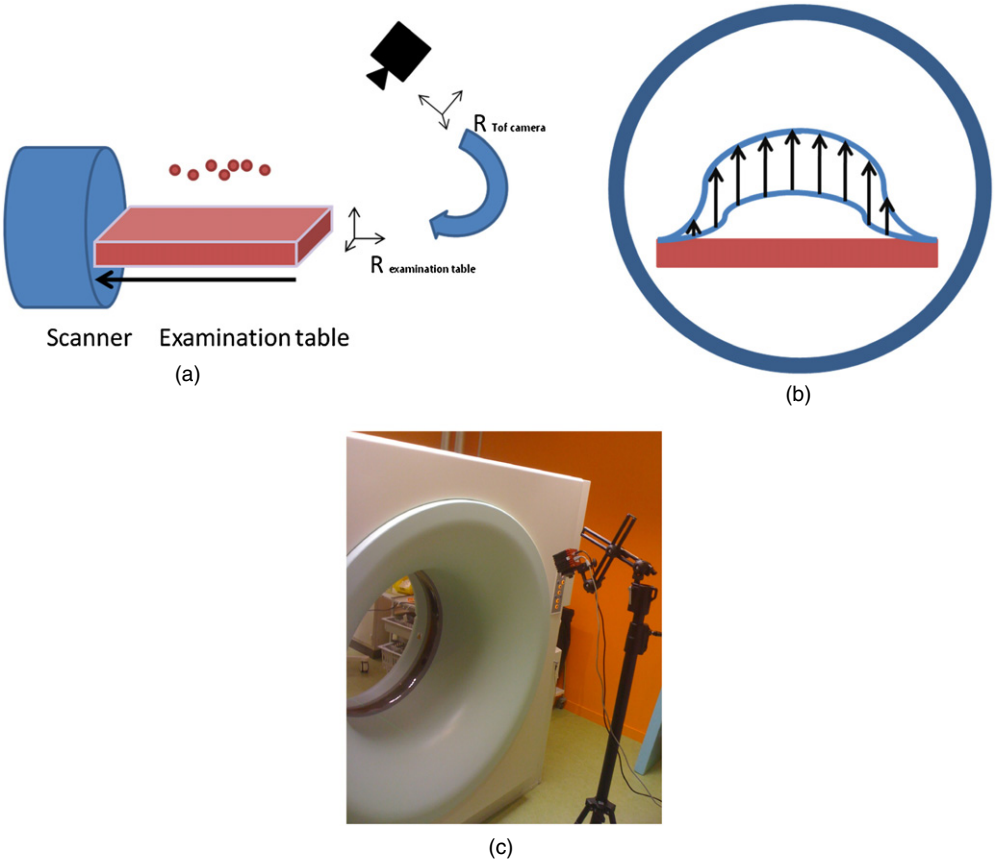

Figure 3. ToF camera acquisition setup showing (a) the spatial reference frame transform from the ToF camera reference to the table, (b) representation of the surface motion from the scanner's axial field of view and (c) during the clinical CT acquisitions.

$F'_{i,j}$ and $F'_{i,j+1}$ associated with each point, the extraction of n' regularly distributed 1D motion vectors between the two B-spline models associated with each set can be computed using

$$\vec{T_i} = \begin{Bmatrix} x_{i,j+1} - x_{i,j} \\ y_{i,j+1} - y_{i,j} \\ F'_{i,j+1} - F'_{i,j} \end{Bmatrix} = \begin{Bmatrix} 0 \\ 0 \\ F'_{i,j+1} - F'_{i,j} \end{Bmatrix}. \tag{3}$$

The number of points can be tuned by setting the resolution of the control grid and/or the application of spatial and temporal averaging. The algorithm is based on the work of Lee *et al* (1997) and makes use of a 'coarse-to-fine' hierarchy of control lattices in order to finally describe the interpolation function as a sum of bi-cubic B-spline functions. The algorithm applies B-spline refinement to the control lattice hierarchy to improve computational time allowing for real-time data processing. In this work, the control point grid for the B-spline modeling was fixed at a 1 cm resolution in x and y directions, in order to ensure that each B-spline grid control point is influenced by multiple measured points.

The algorithm described in this work is suitable for parallelization because the contribution of each measurement point to the B-spline functions is computed independently of the other measurement points. Therefore in multi-core architectures, each core handles a subset of

measurement points in parallel to compute the subset contribution, while all values are gathered to the main CPU in order to update the final B-spline function. While the non-parallel version of the algorithm required 200 ms for the proposed surface modeling running on an AMD Athlon^{TM} 64 X2 dual core processor, the same algorithm running in a multi-thread fashion on an Intel Core 2 Quad 3 GHz processor leads to an execution time of 70 ms.

2.3. Experimental setup and evaluation metrics

The first part of this study aimed at quantifying the improvement of both motion estimation accuracy and repeatability using the B-spline modeling over the use of ToF camera raw measurements. The performance of the ToF camera was investigated through acquisitions carried out using a rigid anthropomorphic surface phantom. Although it allows only rigid motion and its reflectivity is not exactly the same as human skin, the shape of the phantom surface allows realistic observation conditions for the purpose of accuracy and repeatability assessment. Measurements were performed without any motion and with a regular 2 cm translational motion for the repeatability and the relative accuracy of the motion estimation and angularity study, respectively. The motion was performed with the torso phantom placed on a linear actuator capable of generating the specified motion with a guaranteed positioning repeatability of ± 0.02 mm. The camera acquisitions were carried out in real time with a 2 Hz acquisition rate (see section 2.1). Different distances (0.6–1.4 m) and angles (0°, 5°, 10°, 20°, 30°, 35° and 45°) between the camera and the observed surface motion were considered in the evaluation. Observations at different angles were included to evaluate the motion estimation accuracy performance when the camera cannot be placed directly in front of the patient, for example when different radiotherapy or imaging system architectures do not allow it.

A last experiment was performed in order to measure the motion estimation accuracy in the different directions that the proposed surface modeling with B-spline functions allows. Intuitively following a single control point on the modeled surface will allow the detection of motion only along the ToF camera's z-axis. However considering the control point modeling, the entire surface or parts of it should allow recovering the motion in all directions. The anthropomorphic phantom was mounted on two linear actuators allowing an elliptical motion in the x–y plane (major and minor axes of 5 and 3 cm, respectively) and surfaces at eight potions along this path were captured. A feature on the anthropomorphic phantom corresponding to the left pectoral summit was identified, and extracted at each of the eight observed surfaces, by measuring the gradients between the four neighboring control points covering this region. The location of this feature was then compared to the theoretical motion provided by the linear actuators.

On the one hand, the motion estimation accuracy was assessed by measuring the error in quantifying the motion difference between each acquired surface frame and the one considered as the reference in clinically realistic amplitude motion conditions. On the other hand, the repeatability of the motion estimation was assessed by quantifying the variability with which the motion can be estimated under constant motion conditions. For this purpose, a static surface was observed 1000 times and the nonexistent motion was estimated for each pair of consecutive observations. As the real motion was null (since the surface was static), the actual measured surface displacement constitutes a quantification of the motion estimation error as well as the achievable repeatability of this measure. The results were produced for three types of data. The raw measurement points (dataset A), the control points associated with the surface B-spline modeling (dataset B) and dataset B with additional spatial Gaussian filtering applied to the control points (dataset C). The minimum applicable Gaussian filtering of 3×3 was used throughout this work. This filtering was applied considering each control

point of the B-spline surface and its eight neighbors. On the one hand, we emphasize that only datasets B and C were considered in the motion estimation accuracy measurements when actual motion was generated, since an explicit relationship between raw measurement points (dataset A) associated with successive frames does not exist without the proposed surface B-spline modeling (see section 2.2). On the other hand, the repeatability can also be assessed with raw measurements (dataset A) since the surface is not moving and it is therefore possible to associate raw measurement points of each successive frame acquisition to a spatial coordinate. Whiskers' plots were used (MedCalc^{TM} software, Belgium) to represent the mean motion estimation error along the entire surface, quantifying the homogeneity of this estimation along the surface. Finally, we also analyzed the distribution of motion estimation at a single point level. This local assessment is provided by the median error considering all control points.

2.4. Clinical feasibility study

The second part of this study investigated the correlation between a patient's surface motion during a respiratory cycle extracted from 4D CT and the one characterized from B-splines modeled from the ToF acquisitions. The investigation was carried out on three non-small cell lung cancer patients who underwent a 4D-CT examination. In this study, 4D-CT acquisitions were carried out on a Sensation Open 4D-CT scanner (Siemens Healthcare, Germany). Each slice covers 3 mm in depth with a voxel size of $0.83 \times 0.83 \times 3$ mm^3. During data reconstruction, amplitude binning was performed using the external respiratory signal provided by an Anzai© pressure belt attached above the navel. For the current clinical investigations, the camera is placed at the back of the CT gantry at $\sim$1.8 m from the floor mounted on a tripod which allows monitoring the surface of the patient lying on the scanner's bed (see figure 3(c)). The camera does not need to be placed in the same exact location during different patient acquisitions since a transformation is used during each acquisition in order to relate the reference frame of the camera to that of the examination table (see section 2.2). ToF acquisitions of the patient external surface were carried out during the 4D-CT exam at a 10 Hz frequency (see section 2.1).

Despite the availability of the entire patient surface, the ToF surface acquisitions were analyzed to extract respiratory motion information considering different surface regions and sizes (see figure 4(a)) in order to provide the level of motion accuracy at different local and regional levels. The motion estimation in all of the different regions considered throughout the patient surface was simultaneously available. The surface regions used were the ones that have been previously shown to provide a good correlation between external surface and internal anatomical structure motion (Fayad *et al* 2011). Subsequently, the ToF camera acquisitions were binned in the same way as the 4D-CT acquisitions in order to allow a comparison. A relative 1D respiratory signal was extracted by analyzing the global mean motion of each frame with respect to the first one. The binning was based on the signal amplitude similarly to the 4D-CT binning. Different analyses were subsequently performed using the acquired patient 4D-CT datasets and the corresponding patient surfaces.

The acquired 4D-CT volumes were segmented using a threshold-based segmentation algorithm (Zhou *et al* 2004) and patient surfaces were extracted (Fayad *et al* 2011). Subsequent analyses of the two sets of surfaces were performed using different ROIs. This comparison was focused on the abdominal region where most of the movement was observed (see figure 4(b)). Several ROIs of different sizes ($1 \times 1, 2 \times 3, 6 \times 3, 10 \times 3$ and 20×3 cm^2) within this area were considered for subsequent local analysis during this study (see corresponding red, orange, yellow and green ROIs in figure 4(b)). The 1×1 cm^2 ROI is the smallest part of the surface where motion can be analyzed (i.e. the most locally accessible information) considering the

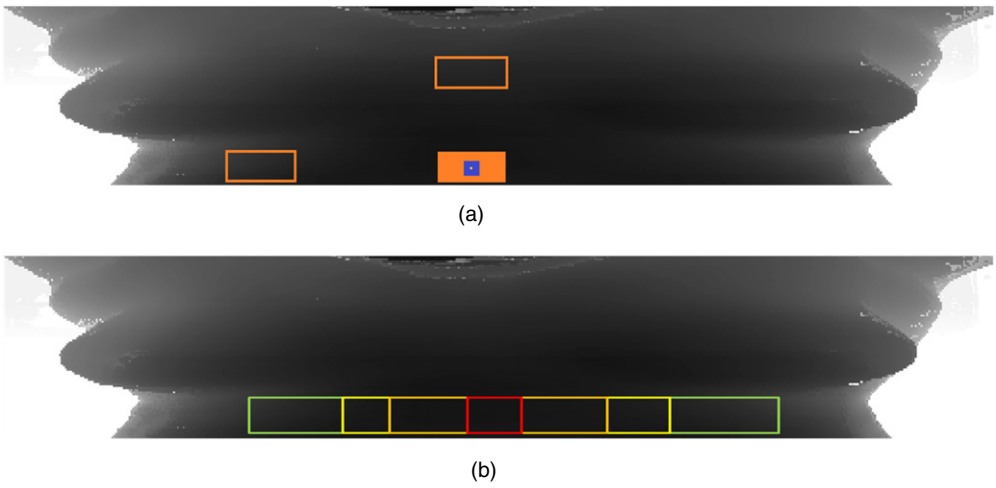

Figure 4. Representation of the different ROIs used (a) to illustrate the impact of region size and location on the respiratory signal quality and (b) for comparison with 4D-CT extracted patient surfaces.

density of the B-spline control points used in the surface B-spline modeling. The mean motion of each ROI for a specific amplitude of the respiratory cycle was computed as the mean motion of all surface voxels of the 4D-CT acquisition (and control points, respectively, for the surface modeled from ToF camera raw data) with respect to the position of the initial surface (at the 0% inspiration phase). Finally, for the largest single area considered (20×3 cm^2), the motion information from ten different ROIs (2×3 cm^2 each) covering this same area was also extracted in order to demonstrate the accuracy in motion monitoring considering multiple ROIs across the same patient surface.

Finally, for one of the acquired patient datasets, respiratory motion modeling was carried out based on the previously proposed principal component analysis (Fayad *et al* 2009). This patient-specific respiratory motion model allows a relationship to be derived between the motion of internal structures and that of external surrogate measures. Internal respiratory motion was calculated using B-spline-based deformable registration between the different 4D-CT frames. Two different surrogate measures were considered for the model creation, on one hand the amplitude of the respiratory motion provided by the pressure belt and on the other the B-spline modeled patient surfaces described in this work. In order to assess its impact, different surrogate measures extracted from the modeled surface were used in the evaluation of the respiratory motion model accuracy. Within this context, and in addition to using the entire modeled surface, different ROI sizes (and numbers) placed over the abdominal region and centered on the umbilicus were also considered. The selected ROI placement area was chosen since it was previously shown to provide the best correlation between external surface and internal structure motion (Fayad *et al* 2011). The CT volumes predicted by the model using the two different external motion surrogate measures have been subsequently compared to their corresponding acquired CT volumes. A clinical expert was asked to select easily identifiable anatomical landmarks in both the acquired and modeled generated CT images (Sarrut *et al* 2006, Fayad *et al* 2011). A total of 13 anatomical landmarks, identified throughout the thoracic field covered by the 4D-CT images and previously used in multiple studies assessing the accuracy of deformable image registration, included the right and left

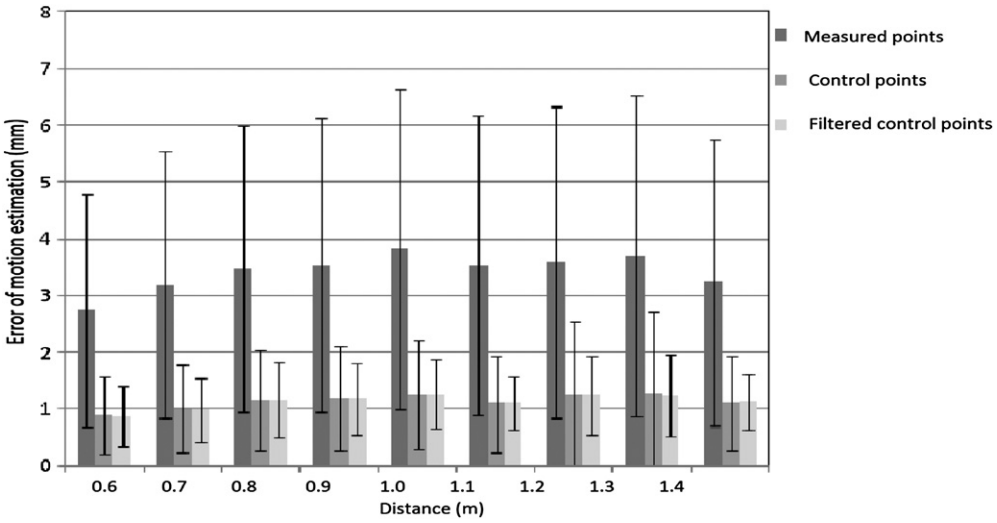

Figure 5. Null (static surface) motion estimation error and associated repeatability (error bars) for different observation distances, considering measured and modeled surface points with and without Gaussian filtering.

apexes, carina, the highest left and right diaphragm positions and the high, low, left and right boundaries of the tumor, covering regions influenced by both large- and small-scale respiratory motion (Giraud *et al* 2003, Van Sörnsen *et al* 2003).

The error between each landmark in the reference and the corresponding model generated CT volumes was subsequently calculated, leading to a model error (ME) given by

$$\mathrm{ME} = \frac{1}{n}\sum_{k=1}^{n}\sqrt{\left(q_x^k - r_x^k\right)^2 + \left(q_y^k - r_y^k\right)^2 + \left(q_z^k - r_z^k\right)^2}, \tag{4}$$

where, q_x^k, q_y^k, q_z^k are the x-, y- and z-coordinates, respectively, of the kth landmark in the acquired CT, and r_x^k, r_x^k, r_x^k are the x-, y- and z-coordinates, respectively, of the kth landmark in the model generated CT. The ME is in millimeters and n is the number of anatomical landmarks.

3. Results

3.1. Phantom experiments

Figure 5 provides the motion estimation accuracy and repeatability results under static conditions for the datasets A, B and C considering the different observation distances varying from 0.6 to 1.4 m. Using raw measurements (dataset A) to characterize the nonexistent motion led to a mean error rising from 2.7 mm at a distance of 60 cm to between 3.2 and 3.8 mm at 1 m and beyond. The associated repeatability as assessed by the standard deviation was poor, with errors up to more than 6 mm. In contrast, the measurement of the null motion was satisfactory using the proposed modeling (datasets B and C), with a mean error of about 1 mm for all distances considered, and good repeatability with a significantly lower standard deviation. More specifically, using the proposed method with additional spatial filtering (dataset C) led to measurements with no error above 2 mm for the entire range of observation distances.

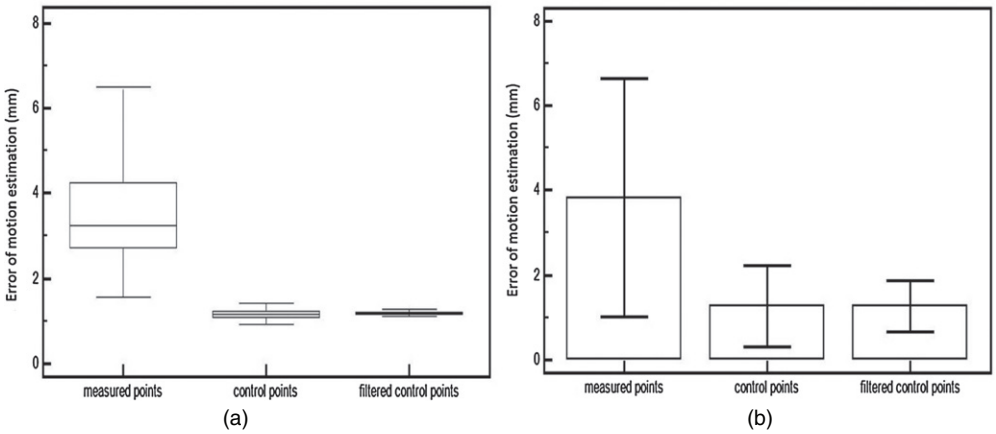

Figure 6. Null (static surface) motion estimation mean error at an observation distance of 1 m when considering (a) the entire surface, and (b) a single surface point (associated with the median error measured in (a)).

Figure 6(a) provides a quantification of the mean motion measurement error and associated variability obtained from the overall surface analysis. Figure 6(b) provides the repeatability for a single surface point chosen as the one associated with the median error among the overall surface. Results of both figures 6(a) and (b) were calculated across the 1000 repeated acquisitions of the static surface for an observation distance of 1 m. The mean motion estimation error for all data describing the surface was 3.6 mm for dataset A and 1.2 mm for datasets B and C (figure 6(a)). As this figure also demonstrates, 95% of the data points are present within an interval of 5.1 mm for A, 0.5 mm for B and 0.3 mm for C, demonstrating that the B-spline modeling allows for a much more homogeneous motion estimation along the observed surface. The repeatability results associated with the single data point analysis as quantified by the standard deviation were 2.8, 1 and 0.6 mm for datasets A, B and C, respectively, demonstrating much more repeatable motion estimation for the proposed method with additional spatial filtering (figure 6(b)).

Figures 7(a) and (b) illustrate the motion estimation error of the moving phantom with respect to increasing observation angle at a fixed observation distance of 1 m, considering the B-spline modeled surface control points without filtering (a) and with filtering (b). Regarding dataset B, the mean motion estimation error for the entire surface was fairly stable with increasing angles of incidence ($\alpha = 0^\circ$–45°). A maximum mean error of 1.2 mm was measured for $\alpha = 30^\circ$. After Gaussian filtering, the mean motion estimation error was measured at 0.7 and 1.1 mm for $\alpha = 0^\circ$ and 45°, respectively, with the error never exceeding 2 mm.

Regarding the orthogonal motion detection considering the elliptical motion pattern at a characteristic point identified on the anthropomorphic phantom surface, the mean error of displacement estimation at this point was 1.2 ± 0.7 mm for the seven positions relative to the initial one.

3.2. Patient acquisitions

Figure 8 shows a comparison of the different respiratory signals recovered from the raw surface measurements and the pressure belt for one of the patient acquisitions. As can been seen in figure 8(a), the respiratory signal corresponding to a single surface pixel, although more noisy,

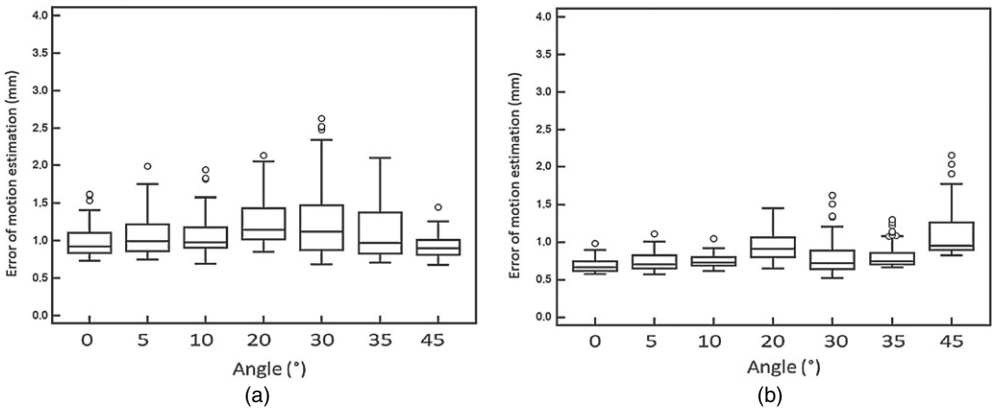

Figure 7. Error of motion estimation for different observation angles considering the entire surface (a) with and (b) without Gaussian filtering.

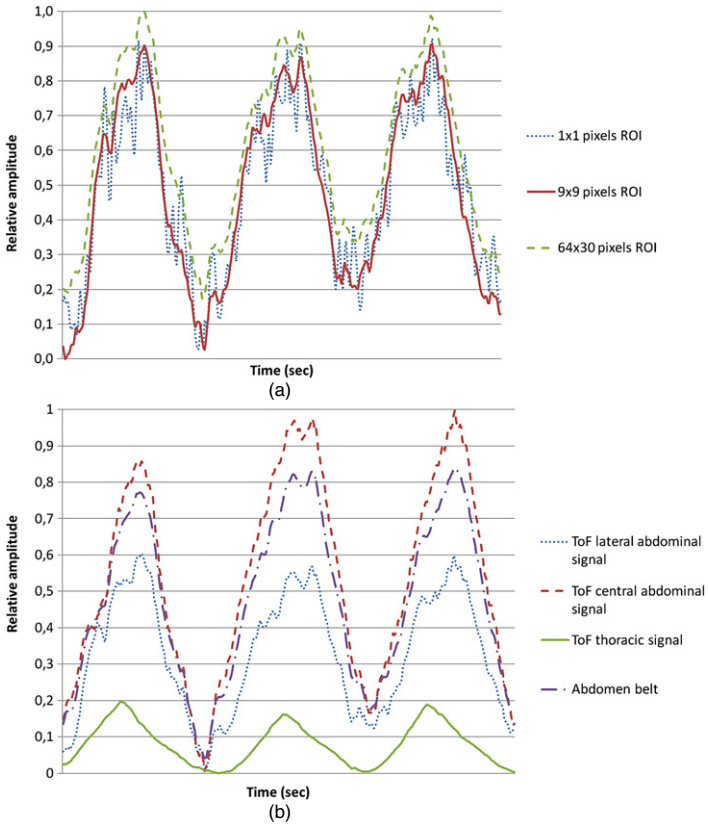

Figure 8. Respiratory signal extracted (a) from the central abdominal area for different ROI sizes shown in figure 4(a) and (b) different ROI locations along the torso (see figure 4(b)).

reveals the same motion pattern compared to larger ROI measurements. On the other hand, figure 8(b) shows for the same patient different amplitude respiratory motion signals extracted from different regions placed throughout the patient surface and the corresponding pressure belt signal.

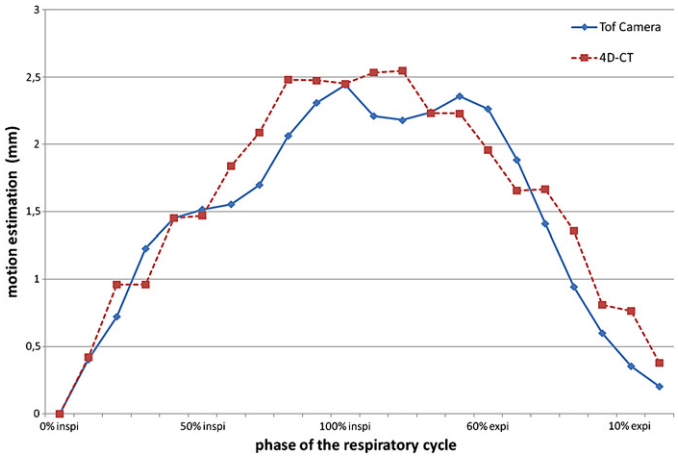

Figure 9. Motion of the 20 $\times$ 3 cm^2 ROI for different phases of the respiratory cycle estimated using the surfaces from the ToF camera and 4D-CT acquisition, respectively, for one of the patient datasets.

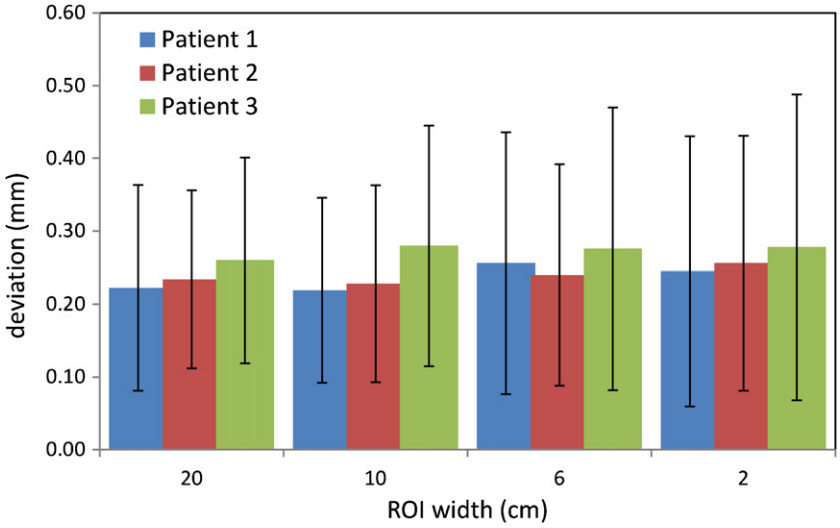

Figure 10. Mean ToF camera-based motion estimation deviation relative to the estimation based on the 4D-CT extracted surfaces for a whole respiratory cycle and different ROI sizes.

Figure 9 illustrates the resulting motion estimation using the proposed approach (B-spline surface modeling with additional spatial filtering) for the 20 $\times$ 3 cm^2 ROI placed in the patients' thoracic region (see figure 4(b)). This estimation is compared to the 4D-CT motion ground truth as determined from the 4D-CT extracted patient surfaces. Through the 21 phases considered, with phase 1 (0% inspiration) taken as a reference position, the mean difference was 0.22 $\pm$ 0.14 mm with a minimum (at 40% inspiration) and maximum (at 80% inspiration) of 0.01 and 0.42 mm, respectively. Results for all three patients are provided in figure 10. Mean

error and associated standard deviation with respect to 4D-CT-derived ground truth rose from 0.24 ± 0.13 mm for a ROI of 20 cm width to 0.26 ± 0.19 mm for a smaller ROI of 2 cm. Considering ten 2 × 3 cm^2 ROIs over the same single 20 × 3 cm^2 region, the corresponding error was 0.25 ± 0.1 6 mm. The mean error and associated standard deviation for the smaller ROI of 1 cm^2 considered was 0.38 ± 0.48 mm. The mean correlation coefficients between the two respiratory signals were 0.75, 0.80, 0.83 and 0.88 for the 2 × 3, 6 × 3, 10 × 3 and 20 × 3 cm^2 ROIs, respectively. No significant differences between the patients were observed, with a robust and accurate estimation of the true motion as determined from 4D CT in all patients, with no mean errors above 0.5 mm.

Finally, considering the evaluation of the patient-specific motion model based on the two different surrogate measures, the use of the surface based on the B-spline model resulted in the smaller mean error of 1.5 ± 0.3 mm compared to a mean error of 3.8 ± 0.6 mm for the use of the amplitude information derived from the pressure belt. This error was 3.8 ± 1.2, 3.6 ± 0.9, 3.3 ± 0.5 and 3.2 ± 0.7 mm for a single ROI of 10 × 1, 6 × 2, 2 × 2 and 1 × 1 cm^2, respectively. This error was reduced to 2.9 ± 0.5 mm when two ROIs of 1 × 1 cm^2 placed over the same region as that covered by the single 2 × 2 cm^2 ROI were used as a surrogate measure.

4. Discussion

The main objective of this study was to investigate the potential of a ToF camera, in terms of both motion estimation repeatability and accuracy improvement through the use of B-spline surface modeling, within the context of real-time patient surface motion monitoring. Respiratory motion synchronization is a necessary process for both imaging and radiotherapy applications reducing the errors in determining organ and tumor locations resulting from involuntary physiological motion. A large variety of patient respiratory motion monitoring devices is available, largely based on the acquisition of a 1D external respiratory signal. Although a comparison of the performance of the proposed approach using the ToF camera to other surface imaging systems (such as structured light or stereoscopic methods) was outside the scope of this work, the ToF camera technology presents a certain number of intrinsic advantages relative to such devices. First, it is marker-less in the sense that it requires no contact with the patient in comparison to the use of external fiducials, optical or magnetic markers, or pressure belt devices that need to be attached to the patient. Second, it allows monitoring the motion of the patient's complete surface, providing a much larger amount of information than 1D respiratory signal. Finally, relative to other systems capable of monitoring a patient's surface, such as those based on structured light or stereoscopic methods, the system is small, light, relatively inexpensive, does not require a calibration step if the range of observation is nearly stable and is able to monitor the entire surface with a frequency of up to 30 Hz. Tarte *et al* (2006) showed that the stereoscopic system VisionRT acquires breathing signals with correlation with spirometer of 0.69 and allows distinction between thoracic and abdominal breathing. Chen *et al* (2010) used colored structured light to measure chest wall motion and estimate respiratory volume with a correlation coefficient $R > 0.99$ with the pneumotachography estimation. Concerning the ToF camera, the main question for the medical applications targeted remains the achievable accuracy, as this technology is designed for fast depth analysis applications which do not require millimeter accuracy.

Before such a potential can be realized, it is necessary to establish in a real-time fashion the spatial relationship between successive camera ToF captures of the moving object, as well as assessing the achievable accuracy and repeatability of such motion measurements. Therefore,

our study focused on determining the performance in terms of repeatability and relative accuracy for this technology with respect to the extraction of patient surface information for the estimation of motion related to respiration when B-spline modeling is applied and used for such motion extraction. A couple of studies have already investigated the use of ToF cameras for patient respiratory motion monitoring. These studies have focused on the correlation between a 1D respiratory signal extracted from the patient surface in comparison with the 1D signal obtained using a pressure belt: correlation coefficients of 0.91 and 0.85 were found for the abdominal and thoracic respiratory signals, respectively (Penne *et al* 2008) and an error of 1.6 $\pm$ 0.2 mm for a plane pseudo-sinusoidal motion observation at 1 m (Clement *et al* 2009). However, these studies did not investigate the potential of this technology to monitor the complete surface motion, neither did they characterize the associated accuracy and repeatability.

In our study a scheme was first proposed allowing a relationship to be established between successive surface captures provided by a ToF camera, considering the absence of anatomical or physical landmarks. This scheme is based on the use of B-spline modeling of the measured surface. First, the results of our study demonstrate that the use of B-spline based modeling allows surface motion monitoring in real time. Although the computational time necessary for modeling the complete acquired patient surface was 200 ms, considering a parallel implementation of the algorithm reduced this time to 70 ms running on an Intel Core 2 Quad 3 GHz processor. This time may be further reduced by code optimization and eventually implementation on GPUs. This is to be contrasted with a mean time of 10 s reported for patient surface motion extraction methods using deformable registration (Schaerer *et al* 2012), which is clearly incompatible with motion management during radiation therapy. On the other hand, the proposed approach allowed a significant improvement on both the motion estimation accuracy and repeatability relative to the raw measurement points. This improvement is substantial with a reduction in the mean motion estimation error from a maximum of 3.8 to 1.3 mm and improved associated repeatability by a factor of $\sim$3 (from 2.8 to 1 mm) for an observation distance of 1 m. In addition, this improvement was not impaired by increasing the observation distance or angle between the object and the ToF camera (evaluated range between 0.6 and 1.4 m and angles between 0° and 45°). However, the absolute motion measurement error did rise with the observation distance (average increase of 40% for both the raw measured and B-spline modeled surfaces for an increasing observation distance from 0.6 to 1 m). For larger observation distances (up to 1.4 m), both the mean error and associated repeatability were stable. This behavior was expected considering that the nominal accuracy provided by the manufacturer follows a similar pattern (i.e. 1% of the distance before 1 m and constant beyond 1 m). When a 3 $\times$ 3 Gaussian filter is applied to the B-spline modeled surfaces, one can observe a motion estimation repeatability improvement for the entire observation distance range, from 22% to 40% for 0.6 and 1.4 m, respectively. Although the impact of the angle of incidence was studied in this work for relative measurements, similar conclusions as Chiabrando *et al* (2010) can be drawn who claimed that there was no significant variation of the distance measurement precision as α changes. In terms of motion detection in a direction orthogonal to the axis of the camera ToF, the use of an elliptical shape motion in combination with the anthropomorphic phantom revealed a mean error of 1.2 mm with extreme errors approaching 2 mm. It is probable that this precision may worsen when one considers the deformable nature of the patient's surface. This accuracy can be only improved by the use of a deformable registration between the successive patient surfaces. However, such an approach will not allow achieving motion monitoring with a frequency of the order of 10 Hz which was achieved in this work.

In a second part, this study investigated the ability of the ToF camera in estimating a real patient respiratory motion, considering therefore all the complex issues not addressed by the phantom experiments, such as the non-rigid nature of motion, and patient skin specific reflectivity or surface variability. Considering the high correlation coefficients obtained between ToF-extracted and 4D-CT-extracted surface motions, the proposed approach allowed an accurate estimation of the patient external motion in a completely non-invasive way. Quantitatively, an accurate estimation of the patients' external breathing motion was provided by analysis of the synchronized 4D-CT acquisitions. The comparison of the motion estimation for various ROIs of different sizes on the torso to their real motion extracted from the corresponding 4D-CT acquisitions as the ground truth showed significant correlation and a good fit of both respiratory signals with a motion estimation difference <0.5 mm. Considering the different ROIs, results showed only a substantial increase ($\sim$50%) of the mean difference regarding the motion estimation, when using a smaller ROI (1×1 cm^2) containing 60 times less pixels (i.e. control points) than the largest one. In addition, the associated standard deviation rose from 0.19 to 0.48 mm, which can be explained by a noisier signal in such smaller areas. These results emphasize that it is possible with this technology and the proposed modeling approach to carry out a local analysis of the respiratory signal as the motion of the smallest area (1×1 cm^2) considered can be accurately characterized with overall errors <1 mm.

Finally, in a single patient the derived motion information using the proposed technology allowed the construction of a more accurate patient-specific motion model. This is in agreement with previously obtained results within the same context using patient external surface motion information derived from patient skin segmentation from acquired 4D-CT images (Fayad *et al* 2009). Relative to the use of the amplitude information from a pressure belt, the surface motion information allowed reducing by over a factor of 2 the mean error in identifying the position of internal structures' motion compared to the acquired 4D-CT images. In addition, we have shown that one can only achieve such substantial improvements in respiratory motion modeling accuracy when considering the use of the entire patient surface based on the proposed B-spline modeling rather than single ROIs placed over a patient's surface. This of course represents a single patient feasibility study and these findings will have to be confirmed in a larger number of patient studies that will be concerned with the evaluation of patient-specific respiratory motion modeling based on external surrogate measures.

Our results suggest a significant potential for the ToF camera technology in combination with the associated modeling approach proposed in this work for real-time respiratory motion monitoring. In addition, the capability offered for local surface motion characterization is clearly an important factor in obtaining an improved correlation between external surface motion with internal organ and tumor motion (Fayad *et al* 2011). The obtained accuracy should be adequate for the purpose of monitoring patient motion in clinical applications such as respiratory synchronization in both imaging and radiotherapy applications. Most importantly, the modeled surface information allows a more accurate patient-specific respiratory motion modeling relative to the use of a single external surface ROI or 1D motion information derived using a pressure belt. The 1.5 mm mean accuracy achieved for the patient-specific motion modeling using the entire surface information may be potentially improved by only considering these parts of the surface which better allow external patient surface and internal anatomical structure correlation (Fayad *et al* 2011). Within this context, the approach previously proposed by Gianoli *et al* (2011) for the combination of different respiratory signals obtained on the patient surface for 4D-CT binning may be adapted for this purpose.

However, one has to note that in this work we constrained the evaluation of this technology at respiratory motion characterization with achievable sampling rates of 10 Hz. Within this

context, we were able to demonstrate errors of <1 and <2 mm in accuracy for absolute motion recovery along the camera's z-axis and in the orthogonal directions, respectively. This accuracy should be sufficient for patient motion management in real time for both imaging and radiotherapy applications. However, continuous patient monitoring during radiotherapy treatment for the detection of non-periodic motion may require higher sampling rates as previously mentioned by Price *et al* who achieved 23 Hz for the entire patient surface. The ultimate challenge will be to combine such sufficiently high rates of entire patient surface capture with a motion modeling approach which does not compromise the real-time aspect delivering absolute motion information. We believe that this may be possible with the B-spline modeling approach implemented on GPU technology and combined with high rate surface capturing devices. Although from a hardware point of view, the camera ToF technology may be capable of achieving such high rate surface monitoring, as described for fast structured light technology by Price *et al*, this has not been tested and evaluated in this work.

In terms of perspectives, the good reproducibility could allow the use of this technology for applications such as patient repositioning in dose fractionation during radiotherapy treatment. The additional information available in terms of monitoring in a real-time fashion the motion of the entire patient surface due to respiration may allow improving both intra- and inter-patient motion modeling. The use of the entire or partial surface instead of a limited area for 1D respiratory signal devices may also be an interesting solution to solve breathing irregularities in 4D-CT reconstruction. The ToF camera technology and associated proposed modeling methodology have the potential to be used in numerous other biomedical applications, including for example head motion monitoring in emission tomography brain studies, imaging of freely moving laboratory animals, or in real-time computer-assisted surgery and/or intra-operative treatment planning.

Different ways to potentially further improve results could be explored, especially concerning two main aspects, namely the quantitative impact of the raw data processing provided by the camera as well as post-processing algorithms. Finally, one of the potential sources of measurement reproducibility errors is the influence of environmental parameters such as background illumination (Kolb *et al* 2010) or the additional light reflected from the 4D-CT gantry. One potential solution to minimize the requirement would be the use of a zoom capable ToF camera technology.

5. Conclusions

Time-of-flight camera technology allows a contact-less whole surface monitoring with acquisition frame rates compatible with the typical patient respiratory cycle. However, the raw surface measurements are associated with significant errors in motion estimation, incompatible with applications in clinical practice. Experiments carried out in this work showed that replacing measured points along these surfaces with spatially filtered control points modeled by B-splines significantly increased the accuracy of surface motion estimation in a robust, reproducible and real-time fashion, which allowed producing promising preliminary results in a feasibility study on patients. ToF cameras may therefore constitute a real alternative for contact-less patient surface monitoring that can be used either in respiratory motion synchronization or modeling for imaging and/or radiotherapy applications. Future work will focus on demonstrating the advantages of using such technology relative to other systems within different clinical settings (motion management in imaging, motion management and patient repositioning in radiotherapy treatment planning).

References

Beddar A S, Kainz K, Briere T M, Tsunashima Y, Pan T, Prado K, Mohan R, Gillin M and Krishnan S 2007 Correlation between internal fiducial tumor motion and external marker motion for liver tumors imaged with 4D-CT *Int. J. Radiat. Oncol. Biol. Phys.* **67** 630–8

Boucher L, Rodrigue S, Lecomte R and Bénard F 2004 Respiratory gating for 3D PET of the thorax : feasibility and initial results *J. Nucl. Med.* **45** 214–9

Brandner E D, Wu A, Chen H, Heron D, Kalnicki S, Komanduri K, Gerszten K, Burton S, Ahmed I and Shou Z 2006 Abdominal organ motion measured using 4D CT *Int. J. Radiat. Oncol. Biol. Phys.* **65** 554–66

Bundschuh R, Martinez-Moeller A, Essler M, Martinez M-J, Nekolla S G, Ziegler S and Schwaiger M 2007 Post acquisition detection of tumor motion in the lung and upper abdomen using list-mode PET data : a feasibility study *J. Nucl. Med.* **48** 758–63

Bussels B, Goethals L, Feron M, Bielen D, Dymarkowski S, Suetens P and Haustermans K 2003 Respiration-induced movement of the upper abdominal organs: a pitfall for the three-dimensional conformal radiation treatment of pancreatic cancer *Radiother. Oncol.* **68** 69–74

Chen H, Cheng Y, Liu D, Zhang X, Zhang J, Que C, Wang G and Fang J 2010 Color structured light system of chest wall motion measurement for respiratory volume evaluation *J. Biomed. Opt.* **15** 026013

Chiabrando F, Piatti D and Rinaudo F 2010 SR-4000 ToF camera: further experimental tests and first applications to metric surveys *Int. Arch. Photogramm. Remote Sens. Spat. Inform. Sci.* **38** 149–54

Clement J-F, Fayad H, Lamard M, Pradier O, Cheze-Le Rest C and Visvikis D 2009 Time of flight camera (TOF) for contact-less and marker-less 3D respiratory motion detection *J. Nucl. Med.* **50** (Suppl. 2) 1541

Dawood M, Büther F, Stegger L, Jiang X, Schober O, Schäfers M and Schäfers K P 2009 Optimal number of respiratory gates in positron emission tomography: a cardiac patient study *Med. Phys.* **36** 1775–84

Falie D, Ichim M and David L 2008 Respiratory motion visualization and the sleep apnea diagnosis with the time of flight (ToF) camera *Proc. of the 1st WSEAS Int. Conf. on Visualization, Imaging and Simulation* pp 179–85

Fayad H, Pan T, Clement J F and Visvikis D 2011 Correlation of respiratory motion between external patient surface and internal anatomical landmarks *Med. Phys.* **38** 3157–64

Fayad H, Pan T, Roux C, Cheze-Le Rest C, Pradier O, Clement J F and Visvikis D 2009 A patient specific model based on 4D CT data and a time of flight camera (TOF) *IEEE Nuclear Science Symp. and Medical Imaging Conf.* pp 2594–8

Gianoli C, Riboldi M, Spadea M F, Travaini L L, Ferrari M, Mei R, Orecchia R and Baroni G 2011 A multiple points method for 4D CT image sorting *Med. Phys.* **38** 656–67

Giraud P, Reboul F, Clippe S, Garcia R, Carrie C, Campana F, Dubray B, Rosenwald J C and Cosset J M 2003 Respiration-gated radiotherapy: current techniques and potential benefits *Cancer Radiothérapie* **7** (Suppl. 1) 15s–25s

Guomundsson S A, Larsen R, Aanaes H, Pardas M and Casas J R 2008 ToF imaging in smart room environments towards improved people tracking *IEEE Computer Society Conf. on Computer Vision and Pattern Recognition Workshops* pp 1–6

Hsu S, Acharya S, Rafii A and New R 2006 Performance of a time-of-flight range camera for intelligent vehicle safety applications *Adv. Microsyst. Autom. Appl.* 205–19

Kanoulas E, Aslam J A, Sharp G C, Berbeco R I, Nishioka S, Shirato H and Jiang S B 2007 Derivation of the tumor position from external respiratory surrogates with periodical updating of the internal/external correlation *Phys. Med. Biol.* **52** 5443–56

Kauweloa K I, Ruan D, Park J C, Sandhu A, Kim G Y, Pawlicki T, Watkins W T, Song B and Song W Y 2012 GateCT^{TM} surface tracking system for respiratory signal reconstruction in 4DCT imaging *Med. Phys.* **39** 492

Kolb A, Barth E, Koch R and Larsen R 2010 Time-of-flight cameras in computer graphics *Comput. Graph. Forum* **29** 141–59

Kubo H and Hill B 1996 Respiration gated radiotherapy treatment: a technical study *Phys. Med. Biol.* **41** 83–91

Lee S, Wolberg G and Shin S Y 1997 Scattered data interpolation with multilevel B-splines *IEEE Trans. Vis. Comput. Graphics* **3** 228–244

Mageras G S, Yorke E, Rosenzweig K, Braban L, Keatley E, Ford E, Leibel S A and Ling C C 2001 Fluoroscopic evaluation of diaphragmatic motion reduction with a respiratory gated radiotherapy system *J. Appl. Clin. Med. Phys.* **2** 191–200

Nehmeh S A *et al* 2004 Quantitation of respiratory motion during 4D-PET/CT acquisition *Med. Phys.* **31** 1333–8

Oggier T, Lehmann M, Kaufmann R, Schweizer M, Richter M, Metzler P, Lang G, Lustenberger F and Blanc N 2004 An all-solid-state optical range camera for 3D real-time imaging with sub-centimeter depth resolution (SwissRangerTM) *Proc. SPIE* **5249** 534–45

Peng J L, Kahler D, Li J G, Samant S, Yan G, Amdur R and Liu C 2010 Characterization of a real-time surface image-guided stereotactic positioning system *Med. Phys.* **37** 5421–33

Penne J, Schaller C, Hornegger J and Kuwert T 2008 Robust real-time 3D respiratory motion detection using time-of-flight cameras *Int. J. Comput. Assist. Radiol. Surg.* **3** 427–431

Plathow C, Ley S, Fink C, Puderbach M, Hosch W, Schmähl A, Debus J and Kauczor H-U 2004 Analysis of intrathoracic tumor mobility during whole breathing cycle by dynamic MRI *Int. J. Radiat. Oncol. Biol. Phys.* **59** 952–9

Price G J, Parkhurst J M, Sharrock P J and Moore C J 2012 Real-time optical measurement of the dynamic body surface for use in guided radiotherapy *Phys. Med. Biol.* **57** 415–36

Sarrut D, Boldea V, Miguet S and Ginestet C 2006 Simulation of 4D CT images from deformable registration between inhale and exhale breath-hold CT scans *Med. Phys.* **33** 605–17

Schaerer J, Fassi A, Riboldi M, Cerveri P, Baroni G and Sarrut D 2012 Multi-dimensional respiratory motion tracking from markerless optical surface imaging based on deformable mesh registration *Phys. Med. Biol.* **57** 357–73

Smith R, Lechleiter K, Malinowski K, Shepard D M, Housley D J, Afghan M, Newell J, Petersen J, Sargent B and Parikh P 2009 Evaluation of linear accelerator gating with real-time electromagnetic tracking *Int. J. Radiat. Oncol. Biol. Phys.* **74** 920–7

Spadea M F, Baroni G, Gierga D P, Turcotte J C, Chen G T and Sharp G C 2011 Evaluation and commissioning of surface based system for respiratory sensing in 4D CT *J. Appl. Clin. Med. Phys.* **12** 3288

SR4000 user's manual 2012 http://www.mesa-imaging.ch/dlm.php?fname=customer/Customer_CD/SR4000_Manual.pdf

Tarte S, McClelland J, Hughes S, Blackall J, Landau D and Hawkes D 2006 A non-contact method for the acquisition of breathing signals that enable distinction between abdominal and thoracic breathing *Radiother. Oncol.* **81** (Suppl. 1) S209

Tsunashima Y, Sakae T, Shioyama Y, Kagei K, Terunuma T, Nohtomi A and Akine Y 2004 Correlation between the respiratory waveform measured using a respiratory sensor and 3D tumor motion in gated radiotherapy *Int. J. Radiat. Oncol. Biol. Phys.* **60** 951–8

Van Sörnsen de Koste J R, Lagerwaard F J, Nijssen-Visser M R, Graveland W J and Senan S 2003 Tumor location cannot predict the mobility of lung tumors: a 3D analysis of data generated from multiple CT scans *Int. J. Radiat. Oncol. Biol. Phys.* **56** 348–54

Vasquez A, Moser T, Gernot E, Sroka-Perez G and Karger C 2009 Investigation of a stereoscopic camera system for gated radiotherapy *IFMBE Proc.* **25** 315–7

Wagman R, Yorke E, Ford E, Giraud P, Mageras G, Minsky B and Rosenzweig K 2003 Reproducibility of organ position with respiratory gating for liver tumors: use in dose-escalation *Int. J. Radiat. Oncol. Biol. Phys.* **55** 659–68

Wu H, Zhao Q, Berbeco R I, Nishioka S, Shirato H and Jiang S B 2008 Gating based on internal/external signals with dynamic correlation updates *Phys. Med. Biol.* **53** 7137–50

Zhou X, Hara T, Fujita H, Yokoyama R, Kiryu T and Hoshi H 2004 Automated segmentations of skin, soft-tissue and skeleton from torso CT images *Proc. SPIE* **5370** 1634–9